Biophysical Chemistry 196 (2015) 40–52

Contents lists available at ScienceDirect

Biophysical Chemistry

journal homepage: http://www.elsevier.com/locate/biophyschem

Investigating the role of GXXXG motifs in helical folding and self-association of plasticins, Gly/Leu-rich antimicrobial peptides ☆

Ludovic Carlier [a,1], Pierre Joanne [b,1], Lucie Khemtémourian [a], Claire Lacombe [a,d], Pierre Nicolas [b], Chahrazade El Amri [b,c,*], Olivier Lequin [a,**]

[a] Sorbonne Universités, UPMC Univ Paris 06, Ecole Normale Supérieure-PSL Research University, Département de chimie, CNRS UMR 7203 Laboratoire des Biomolécules, 4 place Jussieu, F-75005 Paris, France
[b] Sorbonne Universités, UPMC Univ Paris 06, IBPS, Biogenèse des Signaux Peptidiques, 7 quai St Bernard, F-75005 Paris, France
[c] Sorbonne Universités, UPMC Univ Paris 06, CNRS UMR 8256, B2A, Biological Adaptation and Ageing, Integrated Cellular Ageing and Inflammation, Molecular & Functional Enzymology, 7 quai St Bernard, F-75005 Paris, France
[d] Faculté des Sciences et Technologie, Université Paris Est Créteil-Val de Marne, 61 avenue du Général de Gaulle, F-94010 Créteil CEDEX, France

HIGHLIGHTS

- Plasticins have much higher affinity for anionic lipids than zwitterionic lipids.
- The two Gly-rich plasticins fold into well-defined helices in membrane environments.
- In micelles, Gly residues are located on the polar face of the amphipathic helix.
- GXXXG motifs in plasticins do not promote strong association between helices.
- The role of GXXXG motifs in plasticin could differ from that in transmembrane helices.

GRAPHICAL ABSTRACT

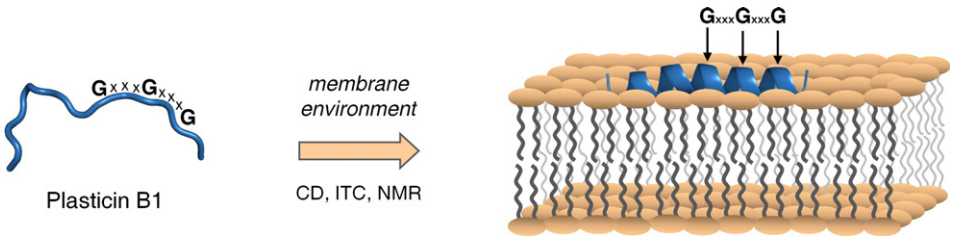

ARTICLE INFO

Article history:
Received 28 July 2014
Received in revised form 16 September 2014
Accepted 19 September 2014
Available online 28 September 2014

Keywords:
Liquid-state NMR
CD
ITC
Cross-linking reaction
Antimicrobial peptide
Membrane mimetics

ABSTRACT

Plasticins (PTC) are dermaseptin-related antimicrobial peptides characterized by a large number of leucine and glycine residues arranged in GXXXG motifs that are often described to promote helix association within biological membranes. We report the structure and interaction properties of two plasticins, PTC-B1 from *Phyllomedusa bicolor* and a cationic analog of PTC-DA1 from *Pachymedusa dacnicolor*, which exhibit membrane-lytic activities on a broad range of microorganisms. Despite a high number of glycine, CD and NMR spectroscopy show that the two plasticins adopt mainly alpha-helical conformations in a wide variety of environments such as trifluoroethanol, detergent micelles and lipid vesicles. In DPC and SDS, plasticins adopt well-defined helices that lie parallel to the micelle surface, all glycine residues being located on the solvent-exposed face. Spectroscopic data and cross-linking experiments indicate that the GXXXG repeats in these amphipathic helices do not provide a strong oligomerization interface, suggesting a different role from GXXXG motifs found in transmembrane helices.

Abbreviations: 1D, one dimensional; 2D, two dimensional; CD, circular dichroism; CSD, chemical shift deviation; DPC, dodecylphosphocholine; DMPC, 1,2-dimyristoyl-*sn*-glycero-3-phosphocholine; DMPG, 1,2-dimyristoyl-*sn*-glycero-3-phospho-1′-*rac*-glycerol; DSS, sodium 2,2-dimethyl-2-silapentane-5-sulfonate; HSQC, heteronuclear single quantum correlation spectroscopy; ITC, isothermal titration calorimetry; LUV, large unilamellar vesicle; MD, molecular dynamics; MLV, multilamellar vesicle; NMR, nuclear magnetic resonance; NOE, nuclear Overhauser effect; NOESY, nuclear Overhauser effect spectroscopy; PBS, phosphate buffered saline; PFG, pulse field gradient; POPG, 1-palmitoyl-2-oleyl-*sn*-glycero-3-phosphoglycerol; PTC, plasticin; RMSD, root mean square deviation; SDS, sodium dodecyl sulfate; TFE, trifluoroethanol; TOCSY, total correlation spectroscopy.

☆ This paper is dedicated to the memory of Francine Bruston, who made significant contributions in the field of plasticins.

* Correspondence to: C. El Amri, UPMC Univ Paris 06, UMR 8256, B2A, Biological Adaptation and Ageing, Integrated Cellular Ageing and Inflammation, Molecular & Functional Enzymology, 7 quai St Bernard, F-75005, Paris, France. Tel.: +33 1 4427 6952.
** Correspondence to: O. Lequin, UPMC Univ Paris 06, Laboratoire des Biomolécules, 4 place Jussieu, F-75005, Paris, France. Tel.: +33 1 4427 3113.
E-mail addresses: chahrazade.el_amri@upmc.fr (C. El Amri), olivier.lequin@upmc.fr (O. Lequin).

[1] LC and PJ contributed equally to this work.

http://dx.doi.org/10.1016/j.bpc.2014.09.004
0301-4622/

1. Introduction

Membrane-active antimicrobial peptides are key elements of innate immunity in most animals, from insects to vertebrates [1,2]. The skin of amphibian, in particular, constitutes a rich source of peptides, with a large number and variety of secreted peptides that can be active on Gram-positive and Gram-negative bacteria, yeasts, fungi and protozoa [3,4]. The isolation and characterization of these antimicrobial peptides has aroused considerable interest with the emergence of numerous microbial strains resistant to conventional antibiotics [5–7].

Plasticins (PTC) are antimicrobial peptides found in the skin secretions of South-American hylid frogs [8,9]. Several members of this family have been identified in species belonging to the genera *Agalychnis*, *Leptodactylus*, *Pachymedusa*, and *Phyllomedusa* [10,11]. These peptides belong to the dermaseptin superfamily of host-defense peptides [12] that are characterized by a strong sequence conservation of signal peptide and precursor proregions but more divergent sequences of the mature peptides [13]. PTCs can be distinguished from other members of the dermaseptin superfamily by a large number of Gly and Leu residues in their sequences [14]. In addition, Gly residues are often arranged in regular 5-mer GXXXG motifs (where X is any amino acid residue). PTCs are typically 23–29 residues in length and contain 1 to 4 GXXXG motifs.

Peptides within PTC family differ markedly in their net charge owing to a different number of positively charged Lys residues, yielding divergent lytic activities. Cationic PTCs such as PTC-B1 isolated from *Phyllomedusa bicolor* and PTC-S1 from *P. sauvagii* exhibit a broad spectrum of antimicrobial activity at micromolar concentrations. In contrast, neutral or weakly cationic PTCs such as PTC-A1 from *Agalychnis annae*, PTC-C1 and PTC-C2 from *A. callidryas*, PTC-DA1 from *Pachymedusa dacnicolor*, and PTC-L1 from *Leptodactylus laticeps* are not potent antimicrobial peptides and tend to be moderately hemolytic. These neutral PTCs may be endowed with other biological properties such as immunomodulation, as demonstrated for PTC-L1 [15], and may act synergistically with other cationic peptides to lyse microorganisms.

The importance of cationic charges in the modulation of biological properties was further demonstrated by incorporating Lys residues in the sequence of neutral PTCs. In particular, we found that substituting three positions in PTC-DA1 by corresponding Lys and Phe residues in PTC-B1 ortholog (Table 1) yielded a cationic peptide [$K^{8,12}$,F^{18}]PTC-DA1 with enhanced antimicrobial potency [10]. The properties of PTC-B1 and the synthetic analog [$K^{8,12}$,F^{18}]PTC-DA1 were extensively studied in order to analyze their interactions with lipids at membrane interfaces and decipher their membrane-disruptive mode of action in relation with their antimicrobial potencies [16–18]. These peptides exhibit differential membrane-lytic activities on a wide range of microorganisms including methicillin-resistant *Staphylococcus aureus* strains [17].

The mode of action of most dermaseptin-related antimicrobial peptides from hylid frogs is believed to be the permeation or disruption of the lipid plasma membrane of the target cells. Several mechanisms have been proposed such as the barrel stave or toroidal pore models, the carpet or detergent models, and the lipid clustering model [19,20]. The involved mechanisms are dependent both on lipid composition and peptide properties with respect to secondary structure, conformational flexibility, charge, hydrophobicity, amphipathicity, and peptide aggregation. Numerous antimicrobial peptides have been reported to adopt amphipathic α-helical structures in membrane environments. Although helical structures have been evidenced for PTC-B1 and [$K^{8,12}$,F^{18}]PTC-DA1 in lipid environments, the conformations adopted by members of the PTC family are markedly dependent on the environment [8]. Indeed PTCs can display random coil, α-helical, β-sheet or β-hairpin structures, revealing their huge conformational plasticity. The large number of Gly residues, which have inherent flexibility, could be an important element of this structural versatility.

Another intriguing property of PTCs is the presence of repeated GXXXG motifs. To this respect, the amino acid sequences of PTCs resemble those of transmembrane protein segments, in which GXXXG motifs are known to mediate interactions between transmembrane helices and promote helix bundle formation [21–23]. GXXXG motifs are prevalent in membrane proteins but they are also observed in soluble proteins in which they can participate in helix-helix interactions [24]. Since peptide self-association is a prerequisite in several proposed mechanisms of membrane permeation, these GXXXG motifs could be involved in peptide oligomerization. Indeed, it has previously been proposed that the central GXXXG motif of PGLa antimicrobial peptide is involved in the formation of an antiparallel helix dimer in the membrane-embedded tilted T-state [25,26]. Other antimicrobial peptides containing GXXXG or AXXXA motifs such as bacteriocins [27] or bombinins [28] also exhibit oligomerization properties. Nevertheless, in the case of PTCs, the involvement of GXXXG motifs in helical bundle formation has not been investigated so far.

The aim of the present work was to analyze the interactions and the conformations of two selected PTCs, PTC-B1 and [$K^{8,12}$,F^{18}]PTC-DA1 analog, in membrane-mimetic environments using ITC, CD and NMR spectroscopy. In particular, we examined to which extent the high number of Gly residues could influence helical folding of PTCs. We also investigated whether the presence of three repeated GXXXG motifs in the two PTCs sequences (Table 1) could promote their self-association in membrane environments.

2. Experimental

2.1. Solid phase peptide synthesis

Peptides (0.1 mmol) were synthesized using FastMoc chemistry on an Applied Biosystems 433A automated peptide synthesizer (Applera, France) as described [10]. Briefly, PTC-B1 was prepared on a Fmoc-Ser(*t*Bu)-Novasyn TGA resin substituted at 0.22 mmol/g (Novabiochem-Merck, Germany). [$K^{8,12}$,F^{18}]PTC-DA1 was synthesized using Rink amide MBHA PS resin substituted at 0.85 mmol/g (Senn Chemicals). Amino acids were purchased from Novabiochem. Peptides were purified by reverse-phase high performance liquid chromatography (RP-HPLC) on a semi-preparative C18 column and their identity and purity were assessed by MALDI-TOF mass spectrometry. Synthesis and purification were performed by the Platform "Synthèse peptidique" of IBPS/FR 3631 Institut de Biologie Paris-Seine (Université Pierre et Marie Curie, Paris).

Table 1
Amino acid sequence and physicochemical characteristics of plasticins investigated in this study.

Peptide[a]	Sequence[b]	Net charge[c]	Mean hydrophobicity[d]	Mean hydrophobic moment (μH)[d]
PTC-B1	GLVTSLIKGA**G**KLL**G**GLF**G**SVT**G**GQS	+2	0.33	3.0
[$K^{8,12}$,F^{18}]PTC-DA1	GVVTDLLKTA**G**KLL**G**NLF**G**SLS**G**-NH_2	+2	0.5	3.96

[a] Plasticins have been renamed according to the new nomenclature proposed by Amiche et al. [9]. PTC-B1 and PTC-DA1 correspond to the formerly named DRP-PBN2 and DRP-PD3-6 peptides, respectively. The analog [$K^{8,12}$,F^{18}]PTC-DA1 was previously called DRP-PD36KF.
[b] Glycines involved in **G**XXX**G** motifs are indicated in bold.
[c] The net charge of the plasticins is given for pH 7.
[d] Mean hydrophobicities and hydrophobic moments (using the CSS scale) were calculated using HydroMCalc program (http://www.bbcm.univ.trieste.it/~tossi/HydroCalc/HydroMCalc.html).

2.2. Preparation of LUVs

1,2-dimyristoyl-*sn*-glycero-3-phosphocholine (DMPC) and 1,2-dimyristoyl-*sn*-glycero-3-phospho-1′-*rac*-glycerol (DMPG) were obtained from Avanti Polar Lipids (Alabaster, AL, USA) and used without further purification. Lipid films were made by dissolving the desired lipids in chloroform for DMPC, or in chloroform/methanol 3:1 for DMPG. The solvent was evaporated under dry nitrogen gas. The resulting films were then kept under vacuum desiccator for at least 30 minutes. Films were then rehydrated with appropriate buffer (10 mM Tris-HCl, 100 mM NaCl, 2 mM EDTA, pH 7.4 for ITC experiments and 10 mM phosphate, pH 7.4 for CD experiments). Lipid suspensions were subjected to 10 freeze-thaw cycles, at temperatures of approximately −190 °C and 50 °C, respectively, and subsequently extruded 19 times through a mini-extruder (Avanti Alabaster, AL) equipped with polycarbonate membranes (200 nm cut-off). The phospholipid content of lipid stock solutions and vesicle preparations was determined by assessing inorganic phosphate according to Rouser [29].

2.3. Circular dichroism

CD spectra were acquired on a Jasco J-810 spectropolarimeter (Jasco Corp., Tokyo, Japan) over the wavelength range 190–260 nm, by using a 0.1-cm path-length quartz cell (internal volume 200 μL) from Hellma (Mullheim, Germany). Spectral measurements were carried out at 25 °C, with a 1 nm/min scan speed and a band width of 1 nm. Plasticin peptides were dissolved in water and immediately diluted in samples containing 30% TFE, 10 mM detergent (DPC or SDS), 1.5 mM DMPC LUVs, or DMPG LUVs. Peptide concentration was 30 μM in all the samples, and measurements in the presence of lipids were performed with a peptide/lipid molar ratio of 1/50. Five scans were accumulated and averaged for each sample. All spectra were corrected by subtraction of the background obtained for each peptide-free mixture. Circular dichroism measurements are reported as $\Delta\varepsilon$ (M^{-1} cm^{-1}) per residue. The relative helix content was estimated according to the relation % helix $= -10 \times \Delta\varepsilon_{222nm}$ [30], where $\Delta\varepsilon_{222nm}$ is the dichroic increment per residue measured at 222 nm.

2.4. Isothermal calorimetry

ITC experiments were performed on a TA instrument nano ITC calorimeter at 25 °C in a buffer containing 10 mM Tris-HCl pH 7.4, 100 mM NaCl, and 2 mM EDTA. Titrations were carried out by injecting aliquots of LUVs (7.5 mM DMPC or 1.5 mM DMPG) into the calorimeter cell containing the peptide solution (peptide concentration between 15 μM and 25 μM), with 5 min waiting between injections. Heats of vesicle dilution were measured by titrating a buffer solution with either 7.5 mM DMPC or 1.5 mM DMPG LUVs under identical conditions. Thermodynamic parameters were determined by non-linear least-square fitting of the buffer-corrected data using the program NanoAnalyze provided by TA Instruments.

2.5. NMR spectroscopy

Peptides were solubilized at a concentration of 1 mM in 550 μL of H_2O/D_2O (90:10 v/v) or H_2O/D_2O/TFE-d_3 (60:10:30 v/v). SDS-d_{25} or DPC-d_{38} detergents (Eurisotop, Saint-Aubain, France) were added at a concentration of 80 mM in H_2O/D_2O samples to ensure a ratio of at least 1 micelle per peptide (assuming an average aggregation number of ~60 detergent molecules per micelle). Sodium 2,2-dimethyl-2-silapentane-d_6-5-sulfonate (Sigma Aldrich) was used as an internal reference (0.1 mM) for chemical shift calibration. The NMR experiments were recorded at 30 °C on a Bruker Avance III spectrometer equipped with a TCI cryoprobe and operating at a ^{1}H frequency of 500 MHz. NMR experiments were processed with Bruker TOPSPIN 2.0 program and analyzed with XEASY [31] or SPARKY [32] programs. ^{1}H and ^{13}C assignments were obtained from the analysis of 2D ^{1}H–^{1}H TOCSY (23 and 69 ms mixing times), 2D ^{1}H–^{1}H NOESY (50 and 100 ms mixing times) and 2D ^{1}H–^{13}C HSQC spectra. The chemical shift deviations (CSDs) of ^{1}H and ^{13}C resonances were calculated using a set of random coil values reported in water [33]. $^3J_{HN-H\alpha}$ and $^3J_{H\alpha-H\beta}$ coupling constants were measured on F_2 rows selected from 2D TOCSY spectra. $^3J_{HN-H\alpha}$ coupling constants were extracted using the INFIT program [34].

2.5.1. Translational diffusion coefficient measurements

The bipolar phase longitudinal encode decode (BPP-LED) sequence developed by Johnson and coworkers [35] was used for diffusion experiments. NMR samples containing 1 mM peptide in the absence or presence of 80 mM detergent (SDS-d_{25} or DPC-d_{38}) were lyophilized and dissolved in 100% D_2O. A low-power presaturation was inserted at the beginning of the pulse sequence for water suppression. For each sample, a series of thirty BPP-LED experiments were recorded at 30 °C with increasing gradient strength from 2 to 95% of the maximum strength (55 G cm^{-1}). This procedure resulted in a series of ^{1}H spectra with decreasing signal intensity according to Eq. (1):

$$I = I_0 \cdot \exp\left[-D.\gamma^2.g^2.\delta^2.(\Delta-\delta/3)\right] \quad (1)$$

where I is the observed signal intensity, I_0 is the signal intensity for zero gradient strength, D is the translational diffusion coefficient, γ is the ^{1}H gyromagnetic ratio, g is the gradient strength, δ is the gradient duration (3.5 ms), and Δ is the diffusion time (100 ms). The DOSY module of NMRPipe [36] was used to calculate diffusion coefficients by fitting Eq. (1) with D and I_0 as adjustable parameters. To determine I values, each spectrum was integrated in a specific region that do not contain overlapping signals from more than one component.

In the case of a peptide/micelle complex, the observed diffusion coefficient of the peptide (D_{obs}) has been shown to be the weighted average of the diffusion coefficients of the bound (D_{bound}) and unbound (D_{free}) species [37,38]:

$$D_{obs} = MF_{bound} \cdot D_{bound} + MF_{free} \cdot D_{free} \quad (2)$$

where MF_{free} and MF_{bound} are the mole fractions of the free and bound peptides, respectively. D_{free} was obtained by measuring the diffusion coefficient of the peptide in the absence of detergent. D_{bound} is generally assumed to be equal to the diffusion rate of the micelle in the presence of peptide [39] and was measured from the detergent resonances using samples containing 1 mM peptide and 80 mM of protonated DPC or SDS. In micellar environment, the diffusion of the free peptide in the aqueous solution is hindered by the presence of the micelles. Therefore, it is important to correct D_{free} by introducing an obstruction factor [37,38] such as:

$$<A> = 1/(1 + 0.5\phi) \quad (3)$$

$$\text{and} \quad D^{\phi}_{free} = D_{free}<A> \quad (4)$$

where ϕ is the volume fraction of the obstructing particles and $<A>$ is a correction factor for spherical objects. This factor has been calculated by Whitehead and co-workers [39] for a 100 mM SDS solution at 25 °C and gave $<A> = 0.96$. Rearrangement of Eq. (2) using D^{ϕ}_{free} allows for the calculation of the mole fraction of micelle-bound peptide (MF_{bound}):

$$MF_{bound} = \left(D_{obs} - D^{\phi}_{free}\right) / \left(D_{bound} - D^{\phi}_{free}\right) \quad (5)$$

2.5.2. NMR positioning experiments

Paramagnetic relaxation enhancements were measured using the micellar samples of plasticins (1 mM in 80 mM detergent) before and after addition of 1 mM gadodiamide (GE Healthcare). The T_1 relaxation

times of Hα protons were measured using an inversion-recovery block implemented at the beginning of a 2D TOCSY sequence (MLEV-17 isotropic sequence of 25 ms duration). A Q3 pulse of 3 ms was chosen for selective inversion of Hα protons after a relaxation delay of 3.5 s. Solvent signal was suppressed with an excitation sculpting scheme prior to acquisition. A set of 12 inversion-recovery 2D TOCSY experiments was recorded in an interleaved manner with inversion-recovery delays varying between 10 ms and 3.5 s. The NMRPipe software [36] was used to process and analyze experiments, and measure cross-peak intensities. T_1 relaxation times were calculated using the non-linear least squares fitting program CurveFit.

2.6. Structure calculation

Interproton distance restraints were estimated from manually assigned NOEs. NOESY cross-peak volumes were measured using XEASY program and four upper limit classes of 2.8, 3.3, 3.8, and 5.0 Å were defined. No hydrogen bond restraints were applied in the calculation. The TALOS + [40] and TALOS-N [41] programs were used to derive backbone dihedral angle restraints based on $^{13}C^{\alpha}$, $^{13}C^{\beta}$, $^{1}H^{N}$ and $^{1}H^{\alpha}$ chemical shifts analysis. The ϕ, ψ torsion angles of residues that were consistently predicted to fall into the α_R region of the Ramachandran map were restrained around $-60° \pm 30°$ and $-40° \pm 30°$, respectively. Additional (ϕ, ψ) restraints were defined around ($-75° \pm 45°$, $-20° \pm 50°$) for a few residues "generously" predicted in helical conformation by both TALOS + and TALOS-N programs. A set of 100 structures was calculated by torsion angle dynamics in DYANA using standard parameters [42]. The best 25 structures having the lowest target function were then minimized using the XPLOR-NIH program [43] and CHARMM22 force field. Nonbond terms consisted of a Lennard-Jones potential and an electrostatic potential with a distance-dependent dielectric model ($\varepsilon = 4r$) to mimic the presence of solvent. The 20 structures exhibiting the lowest energies were selected to represent the NMR ensemble. Structures were analyzed using InsightII (Accelrys, San Diego, CA) and PROCHECK-NMR programs [44].

2.7. Cross-linking assays and Tris-Tricine SDS-PAGE

Plasticin peptides were diluted in PBS (Life Technologies, containing 8 mM Na_2HPO_4, 1.5 mM KH_2PO_4, 138 mM NaCl, 2.7 mM KCl) at 100 μM concentration and incubated during 30 minutes at room temperature in the presence of 10 mM detergents (DPC or SDS) or 5 mM LUVs (DMPC or DMPG). Then 0.15 % glutaraldehyde was added and solutions were kept at room temperature during 60 minutes. The cross-linking reaction was stopped by addition of 0.1 M Tris-HCl. Solutions were then diluted with an equal volume of loading buffer (0.2 M Tris, 2% SDS, 2% β-mercaptoethanol, 40% glycerol, 0.04% Coomassie Brilliant Blue G-250, pH = 6.8), boiled at 95 °C, and deposited on a 10–20% Mini-PROTEAN® Tris-Tricine gel (Biorad). Migration was run at 75 V during 5 hours at 4 °C in Tris-Tricine buffer (0.1 M Tris, 0.1 M Tricine, 0.1% SDS). After migration, gels were incubated during 30 min with the fixative solution (40% methanol and 10% acid acetic) and stained during 60 min with 0.25 g/L Coomassie blue G-250 in 10% acetic acid. Gels were rinsed with 10% acetic acid until bands were clearly visible.

3. Results

3.1. Influence of membrane environments on the secondary structure of plasticins inferred from CD spectroscopy

Most antimicrobial peptides are unstructured in aqueous solution and tend to adopt a well-defined secondary structure when in contact with lipid membranes. To investigate the influence of membrane environments on the structure of the two plasticins, we first recorded far-UV CD spectra in the absence and presence of large unilamellar vesicles (LUVs) made of zwitterionic or anionic phospholipids (DMPC and DMPG, respectively). Because the outer leaflet of bacterial membranes is composed mainly of anionic lipids, DMPG was chosen as a model system of bacterial membranes, while DMPC is more representative of mammalian cell membranes. As shown in Fig. 1, the CD spectra of both peptides in aqueous solution display a single negative band near 200 nm, indicative of random coil conformation. In contrast, the two plasticins adopt an α-helical conformation in the presence of phospholipids, as inferred from the two intense negative bands observed around 208 and 222 nm with both zwitterionic and anionic vesicles. The helical content, estimated from the ellipticity value at 222 nm [30], is significantly higher in the presence of anionic vesicles for both peptides, ranging from 44–58% with DMPC to 66–80% with DMPG. These results indicate that the two PTCs interact with both zwitterionic and anionic membranes, and that electrostatic interactions between the two Lys residues of PTCs and the negatively charged lipids provide additional stabilization in helical folding.

CD spectra were also recorded in the presence of 30% trifluoroethanol (TFE) and two detergent micelles (DPC and SDS), these environments being compatible with high-resolution solution NMR studies (see below). In the case of [$K^{8,12}$,F^{18}]PTC-DA1, the CD spectra acquired in TFE, SDS, and DPC are highly similar to the one obtained in DMPG, ellipticity values being consistent with helical contents of 71–79%. These three media also induce an α-helical conformation of PTC-B1 structure but with weaker helical contents (57–61%) in comparison to [$K^{8,12}$,F^{18}] PTC-DA1. Overall, PTC-B1 appears to be more flexible than [$K^{8,12}$,F^{18}] PTC-DA1 in all the membrane environments used in this study. The CD data also reveal that the nature of the detergent polar headgroup has little influence on the secondary structure of both plasticins, indicating that the main driving force is the sequestration of hydrophobic residues at the micelle/water interface.

3.2. Thermodynamic analysis of the interaction between plasticins and lipid vesicles

ITC was used to gain insight into the binding mode of the two plasticins with zwitterionic and anionic vesicles. Binding isotherms were obtained by injecting either DMPC or DMPG LUVs into the calorimeter cell containing a plasticin solution at 25 °C. On this basis, the enthalpy of binding of the peptide to the liposome (ΔH) was determined as well as the binding constant K_A. The dissociation constant K_D, the Gibbs free energy (ΔG) and the entropy (ΔS) of binding were derived from K_A and ΔH. As shown in Fig. 2A and C, the titrations of PTC-B1 and [$K^{8,12}$,F^{18}]PTC-DA1 with DMPC LUVs led to the observation of exothermic signals, indicating an enthalpy-driven process. The two peptides bind zwitterionic vesicles with a similar affinity in the micromolar range (K_D = 22–25 μM, Table 2). The binding to DMPG LUVs (Fig. 2B and D) gave rise to larger enthalpies which correlate with a 10–50 fold higher affinity for anionic vesicles (K_D = 0.55–1.7 μM). This underlines that electrostatic interactions between Lys residues and anionic lipids at the surface of the bilayer are crucial for membrane selective recognition of the plasticins. Interestingly, the entropic term (−TΔS) contributes to more than 75% of the total free energy of interaction (ΔG) in all the experiments conducted (Table 2). This demonstrates the importance of hydrophobic interactions in the membrane-binding process in addition to electrostatic interactions. Indeed, a large entropy gain is generally ascribed to the release of water molecules from the hydrophobic regions of the bilayer upon peptide incorporation [45,46], resulting in favorable hydrophobic interactions between non-polar residues of the peptides and the membrane core.

It should be stressed that many injection peaks in Fig. 2 exhibit a pronounced shoulder on the right side, suggesting that an additional thermodynamic process distinct from the peptide/lipid interaction is occurring during the titration. Similar appearances of ITC traces have been observed for cell penetrating peptides interacting with POPG LUVs [47] and were interpreted as the result of liposome reorganization. In addition, increasing the peptide concentration in the calorimeter cell from 15–25 μM to

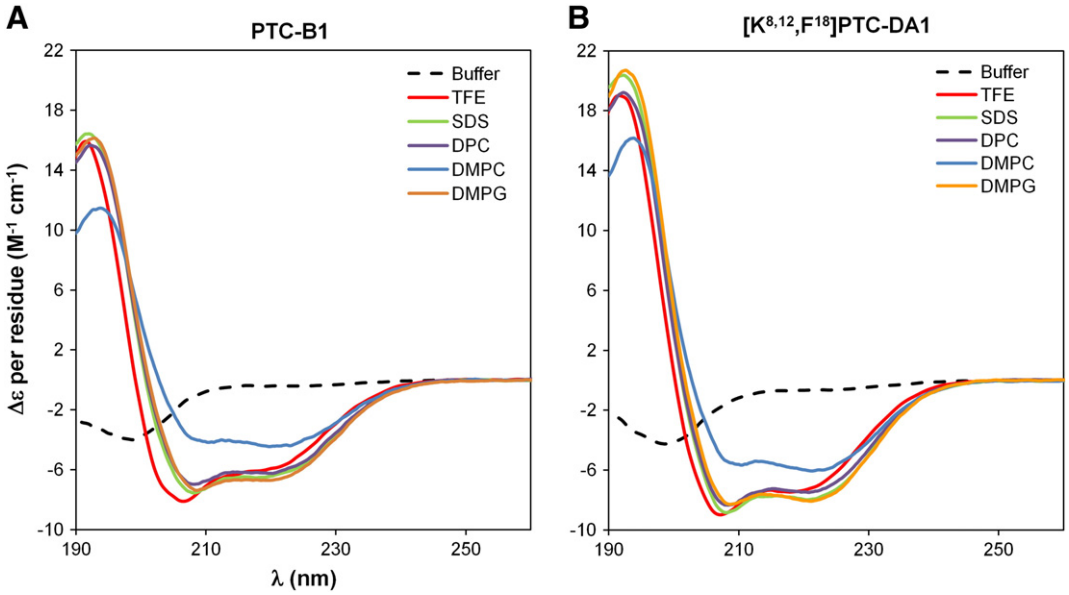

Fig. 1. Far-UV CD spectra of PTC-B1 and [$K^{8,12}$,F^{18}]PTC-DA1 in phosphate buffer, 30% TFE, DPC micelles, SDS micelles, DMPC LUVs, and DMPG LUVs. Spectra were recorded at 25 °C using a peptide concentration of 30 μM.

40–50 μM led to more complex ITC traces with endothermic peaks observed at the beginning of the titration followed by exothermic peaks (data not shown). The presence of additional thermodynamic processes has been shown for other antimicrobial peptides upon vesicle titration, and was proposed to be the result of pore formation, changes in the lipid phase properties, and/or peptide aggregation [46].

3.3. NMR conformational studies of plasticins in membrane-mimetic environments

The conformations of plasticins were further examined at the residue level by solution NMR spectroscopy in three different environments: water/TFE mixture (70:30), zwitterionic DPC, and anionic SDS

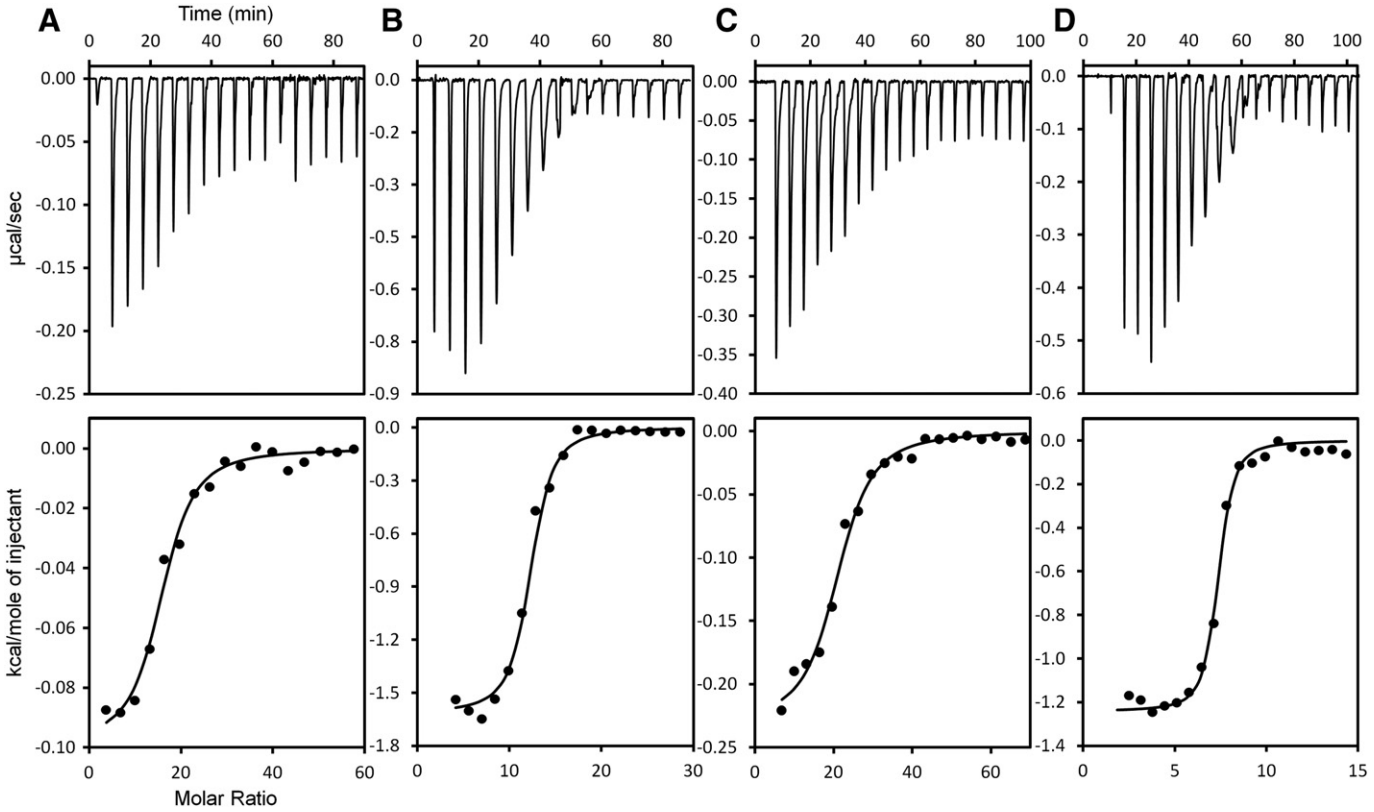

Fig. 2. Isothermal titration of PTC-B1 (A and B) and [$K^{8,12}$,F^{18}]PTC-DA1 (C and D) with DMPC (A and C) or DMPG (B and D) LUVs at 25 °C. The lower curves represent the heat of reaction (measured by peak integration) as a function of lipid/peptide molar ratio. The solid lines represent the best fits to experimental data. Thermodynamic parameters calculated from these experiments are presented in Table 2.

Table 2
Thermodynamic parameters for PTC-B1 and [$K^{8,12}$,F^{18}]PTC-DA1 binding to DMPC or DMPG large unilamellar vesicles (LUVs) at 25 °C.

Peptide	PTC-B1		[$K^{8,12}$,F^{18}]PTC-DA1	
Vesicle type	DMPC	DMPG	DMPC	DMPG
K_A (M^{-1})	4.5 10^4	5.8 10^5	4.0 10^4	1.8 10^6
K_D (μM)	22.0	1.7	24.9	0.55
ΔH (kJ/mol)	−0.41	−6.75	−0.96	−5.19
ΔG (kJ/mol)	−26.6	−32.9	−26.2	−35.7
ΔS (J/mol/K)	87.7	87.6	84.8	100.2
TΔS (kJ/mol)	26.1	26.1	25.3	30.5
Binding stoichiometry (n)	15.1	11.7	20.4	7.1

Table 3
Translational diffusion coefficients (D_{obs}) of the plasticins in the absence and presence of DPC and SDS micelles as determined by PFG-NMR experiments.

	PTC-B1	[$K^{8,12}$,F^{18}]PTC-DA1
D_{obs} in H_2O (10^{-10} m^2 s^{-1})	2.20	2.37
D_{obs} in DPC (10^{-10} m^2 s^{-1})	1.01	0.98
D_{obs} in SDS (10^{-10} m^2 s^{-1})	0.74	0.79
MF_{bound} in DPC[a]	0.78	0.82
MF_{bound} in SDS[a]	0.86	0.85

[a] The mole fractions of micelle-bound peptide (MF_{bound}) were calculated using Eq. (5).

micelles. TFE was chosen as an organic cosolvent in order to assess the intrinsic helical propensity of both peptides in the absence of a water-membrane interface. The use of micelle systems in solution-state NMR studies is a widely used approach to mimic water-membrane interfaces because of the high-quality spectra usually obtained for the solubilized peptides. Although micelles do not form bilayers, they are considered as relevant models to characterize the surface-bound conformation of antimicrobial peptides and probe the initial states of interaction with biological membranes [48,49].

The NMR spectra of plasticins in the different investigated media exhibited overall good quality in terms of chemical shift dispersion and resonance linewidths, demonstrating the folding of peptides and the absence of aggregation. In the case of micellar environments, pulsed field gradient (PFG) NMR experiments were recorded to evaluate the partitioning of both plasticins in DPC and SDS micelles. Indeed, the binding of a peptide to a micelle can be monitored by measuring changes in the translational diffusion coefficient of the peptide because the molecular size of a peptide/micelle complex is significantly higher than that of the free peptide in aqueous solution [37–39]. Since the equilibrium between the free and micelle-bound forms is fast on the NMR time scale, the mole fraction of micelle-bound peptide can be estimated from the observed diffusion coefficient of the peptide, which is the weighted average of the diffusion coefficients of the free and bound species (Eq. (5)). A bipolar pulse longitudinal encode decode (BPP-LED) sequence was used to measure the diffusion coefficients of both plasticins in the absence and presence of detergent. As reported in Table 3, the translational diffusion coefficients of the plasticins dramatically decrease in the presence of DPC and SDS detergents, indicating a strong interaction with both micelle types. The high affinity of the two plasticins for DPC and SDS micelles is confirmed by the mole fraction of micelle-bound peptide (MF_{bound}) which shows that 76 to 86% of the peptides are partitioned in micelles. The partitioning of plasticins appears to be greater in anionic micelles than in zwitterionic counterparts, indicating that electrostatic interactions between the micelle anionic head group and the positively-charged side chains of Lys-8 and Lys-12 slightly enhance the affinity for these membrane mimetics.

3.4. Secondary structure of plasticins probed by NMR conformational parameters

The next step in this analysis was to characterize the secondary structure of the plasticins at the residue level from the NMR conformational parameters. For that purpose, sequence-specific ^1H resonance assignments were obtained for both plasticins in water/TFE and micellar environments from the analysis of through-bond 2D TOCSY and through-space 2D NOESY correlation experiments. Aliphatic ^{13}C resonances were also assigned using 2D natural abundance ^{13}C-^1H HSQC experiments to facilitate side-chain resonance assignments and provide additional conformational parameters. Resonance assignments are provided in the Supplementary Information (Tables S1-S6).

The local conformational preferences of individual residues were first characterized using $^1H\alpha$ and $^{13}C\alpha$ chemical shift deviations (CSDs), which are defined as the differences between experimental chemical shifts and corresponding random coil values for each amino acid [33]. In the three media, most residues of both peptides exhibit downfield shifts of Cα resonances (Fig. 3) and upfield shifts of Hα resonances (not shown) that are indicative of helical conformations, as inferred from CD spectra. CSD values were analyzed in more details to assess the helical propensity of each residue and to delineate the helical segments in the three different media.

The continuous stretch of positive Cα CSD values observed for PTC-B1 in TFE (Fig. 3A) indicates that the helix extends from residues 2 to 21, the C-terminal 22–26 region being mostly unfolded. The two glycine residues at positions 9 and 16 have markedly diminished helical propensities in comparison with nearby residues, and delineate three helical segments of decreasing helical stability from the N to the C-terminus. The interaction with detergent micelles leads to an increase in helical populations in comparison with water/TFE medium, with average Cα CSD values of 2.5 and 2.7 ppm for residues 2–21 in DPC and SDS, respectively, versus 1.7 ppm in water/TFE. Interestingly, the CSD analysis reveals that the profiles of helical propensity along the sequence are similar in TFE and in both detergents (Fig. 3B, C). In particular, the helical propensity of PTC-B1 is the strongest in the N-terminal 2–8 region, decreases in the central 9–15 segment, and is the weakest in the C-terminal part. The main difference between the three media concerns the C-terminal extension of the helix. In DPC micelles, the helix tends to be shorter and is loosened in the 18–21 segment, as shown by gradually decreasing Cα CSD values.

The Cα CSD analysis reveals that [$K^{8,12}$,F^{18}]PTC-DA1 has a higher helical propensity than PTC-B1 in the three investigated media (Fig. 3). This increased helical stabilization with respect to PTC-B1 is observed in TFE most particularly, and in micellar environments to a lesser extent, with average Cα CSD values over the 2–21 segment of 2.7, 2.9 and 3.0 ppm in TFE, DPC and SDS, respectively. As for PTC-B1, the N-terminal segment (residues 2–9) appears to have the highest helical propensity whereas the C-terminal end shows loosening of the helical structure. The length of the helix is also shorter in DPC micelles, as seen for PTC-B1. In contrast, no helix destabilization is observed at positions 9 and 16 that are occupied by non-glycine residues in the case of [$K^{8,12}$,F^{18}]PTC-DA1 peptide.

The helical conformations were further confirmed by the pattern of intraresidual, sequential, and medium-range NOEs showing characteristic $H\alpha_i$–HN_{i+3}, $H\alpha_i$–$H\beta_{i+3}$ and $H\alpha_i$–HN_{i+4} correlations (Supplementary Fig. S1). The $^3J_{HN-H\alpha}$ coupling constant constitutes another interesting conformational probe owing to its dependence over ϕ dihedral angle. Indeed, regular helical conformations typically yield $^3J_{HN-H\alpha}$ values below 5.5 Hz whereas values around 6–7 Hz correspond to distortion from canonical ϕ values or increased disorder. The analysis of $^3J_{HN-H\alpha}$ coupling constants could not be drawn in micellar environments because the observed broadening of amide resonances precluded an accurate measurement. In TFE, most residues of [$K^{8,12}$,F^{18}]PTC-DA1 peptide have coupling constants smaller than 5.5 Hz (Supplementary Table S4), with the exception of Thr9 and the C-terminal Leu21 and Ser22 residues. The increased value for Thr9 could be due to a slight destabilization or deformation of the helix by this β-branched residue. In the case of PTC-B1 (Supplementary Table S1), the N-terminal half

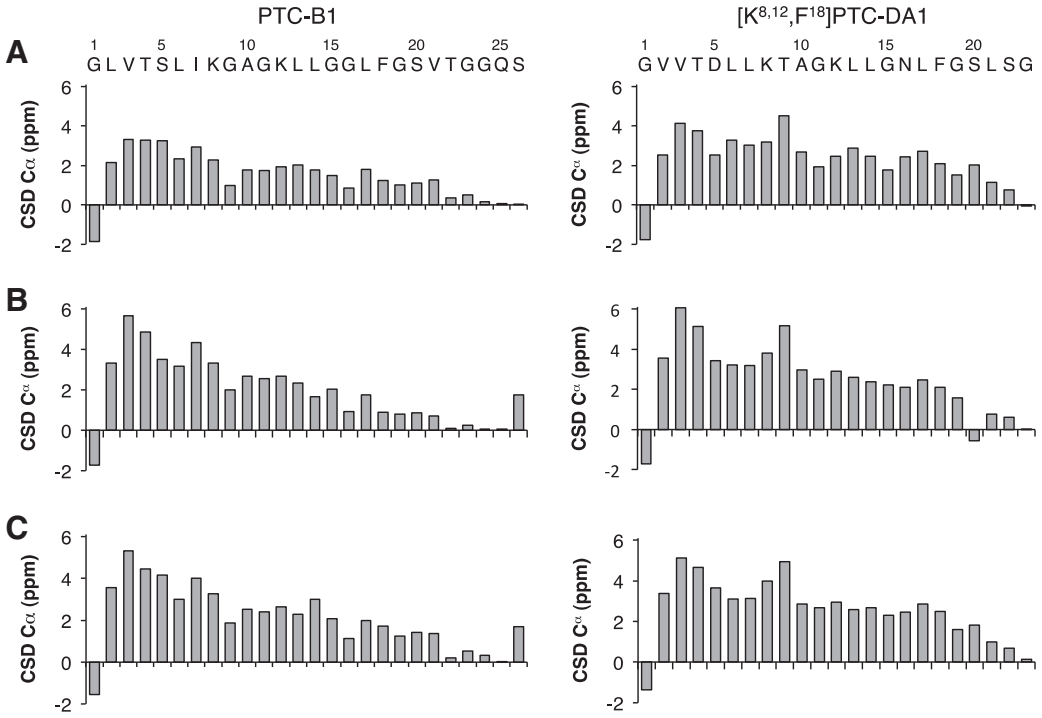

Fig. 3. Chemical shift deviations (CSDs) of Cα resonances for PTC-B1 (left) and [$K^{8,12}$,F^{18}]PTC-DA1 (right) in 30% TFE (A), DPC micelles (B), and SDS micelles (C).

shows the smallest values for the $^{3}J_{HN-H\alpha}$ coupling constants whereas the C-terminal half exhibits increased values, which is in good agreement with the differences in helical stability deduced from both CSD and NOE analysis.

3.5. Three-dimensional structures of plasticins in the different environments

The NMR structures of plasticins were calculated by restrained molecular dynamics with DYANA and refined by energy minimization using XPLOR-NIH and CHARMM22 force field. In addition to distance restraints derived from NOEs, χ1 dihedral angle restraints could be determined from $^{3}J_{H\alpha-H\beta}$ coupling constants measured for several residues (Table 4). Information on ϕ, ψ dihedral angles was derived from the Cα CSD analysis, as aforementioned, and was further confirmed by a deeper analysis of ^{1}HN, ^{1}Hα, ^{13}Cα and ^{13}Cβ chemical shifts based on TALOS + program [40] and the more recent version TALOS-N [41].

The calculated NMR structures have good geometric quality and display few restraint violations (Table 4). The structural definition, measured by backbone rmsd, is also in good agreement with the CSD and NOE analysis. The structures of both plasticins in the three different media (Fig. 4) all form an uninterrupted helix starting at residue 2 but whose length depends on peptide sequence and medium. The helix structure of [$K^{8,12}$,F^{18}]PTC-DA1 tends to be slightly longer than that of PTC-B1 in the three media, the helix of PTC-B1 being the shortest in DPC micelles. The helical structures show increased disorder of the C-terminal residues.

The absence of helix interruption around Gly positions is supported by the NOEs, chemical shifts and J coupling analysis. Interestingly, the structures of PTC-B1 tend to adopt a slight curvature around the third turn of the helix. Inspection of the backbone hydrogen bond networks shows that regular CO_i-HN_{i+4} hydrogen bonds are observed throughout the α-helical structure, except in the 8–12 region. Indeed, the hydrogen bonds involving the carbonyl groups of residues 8 and 9 have increased lengths and a 3_{10}-hydrogen bond is observed between the carbonyl of Gly 9 and amide group of Lys12. This small distortion of the hydrogen bond network does not seem to be imposed by any NMR restraint and is more likely a consequence of the presence of two nearby glycines at positions 9 and 11.

The analysis of side chain distribution reveals that both plasticins adopt amphipathic structures. A large hydrophobic face is formed by Leu residues predominantly together with Ile, Val and Phe residues. These residues display numerous van der Waals interactions as shown by many NOEs involving side-chain protons. Glycine residues are localized on the hydrophilic face of the helix which is formed mostly by the polar side chains of Ser, Thr and the two charged Lys residues.

3.6. Position of plasticins within micelles

The position of plasticin peptides with respect to DPC and SDS micelle surface was further investigated by solution NMR spectroscopy. The use of gadodiamide, a paramagnetic MRI contrast agent, has been considered for several years as one of the most accurate approaches to probe the immersion depth of polypeptides within micelles [50–52]. Gadodiamide is a water-soluble $Gd^{(III)}$ complex that enhances T_1 relaxation rates of protons in a distance-dependent manner. This neutral probe partitions into the aqueous environment outside the micelles and, in contrast to charged paramagnetic agents, has uniform distribution towards peptide-micelle complexes. Therefore, residues that lie outside or close to the micelle surface are expected to exhibit the highest paramagnetic relaxation enhancements (PRE). We quantified the enhancement of Hα protons longitudinal relaxation by inserting a T_1 inversion-recovery block in a 2D TOCSY sequence.

PREs measured for the two plasticin peptides in anionic SDS micelles are shown in Fig. 5A. The gadodiamide probe strongly enhances the relaxation of Hα protons in residues at the C-terminus, indicating that these flexible residues are not buried inside the micelle. A periodicity in the PRE values is apparent in the N-terminal and central parts, and supports that the helical region 2–18 adopts a roughly parallel orientation with respect to the micelle surface in both plasticins. In particular, hydrophobic residues at positions 3, 7, 10 and 14, which lie on the same helical face, display the lowest PREs and are therefore located deep inside the SDS micelle. Overall, the position and orientation of PTC-B1 and [$K^{8,12}$,F^{18}]PTC-DA1 within SDS micelles are almost

Table 4
Structural statistics of NMR structures.

	PTC-B1			[K^{8,12},F^{18}]PTC-DA1		
	TFE	DPC	SDS	TFE	DPC	SDS
Experimental restraints						
Number of NOE-derived distance restraints	162	192	190	174	205	212
Intraresidue	84	84	88	84	84	89
Sequential	69	77	78	73	74	80
Medium-range	9	31	24	16	47	43
Number of dihedral angle restraints	40	37	43	40	38	43
ϕ, ψ	20	16	20	20	18	20
χ1	0	5	3	0	2	3
Number of restraint violations						
Distance violations >0.1 Å	0.1 ± 0.3	3.9 ± 1.3	2.5 ± 0.7	0.6 ± 0.8	4.8 ± 1.2	3.4 ± 1.3
Dihedral angle violations >5°	0.3 ± 0.6	0.2 ± 0.4	0.2 ± 0.5	0	0	0
Rms deviations from experimental restraints						
Distances (pm)	0.8 ± 0.2	2.5 ± 0.2	1.8 ± 0.1	1.1 ± 0.2	2.6 ± 0.2	2.2 ± 0.1
Dihedral angles (°)	0.54 ± 0.46	0.62 ± 0.46	0.73 ± 0.36	0.08 ± 0.14	0.09 ± 0.22	0.19 ± 0.17
Structural statistics						
Rms deviations from ideal covalent geometry						
Bonds (pm)	0.92 ± 0.02	0.86 ± 0.02	0.87 ± 0.02	0.91 ± 0.01	0.89 ± 0.01	0.91 ± 0.02
Angles (°)	1.85 ± 0.04	2.01 ± 0.10	1.93 ± 0.05	1.87 ± 0.05	2.11 ± 0.03	2.07 ± 0.05
Impropers (°)	1.00 ± 0.10	1.32 ± 0.15	1.02 ± 0.14	0.87 ± 0.06	1.22 ± 0.16	1.18 ± 0.09
Van der Waal's energy (kJ.mol^{-1})	−298 ± 17	−270 ± 28	−314 ± 23	−295 ± 9	−283 ± 78	−256 ± 9
MolProbity clash score (Z-score)	1.48	1.48	1.53	1.53	1.53	1.53
Ramachandran plot dispersion (%)						
Most favored regions	92.1	80.9	90.3	94.2	95.0	92.2
Additionally allowed regions	5.9	14.1	7.6	5.6	4.7	6.4
Generously allowed regions	0.9	4.1	0.9	0.0	0	0.6
Disallowed regions	1.2	0.9	1.2	0.3	0.3	0.8
Backbone atoms rms deviation (Å)						
All backbone atoms	2.39	3.73	2.17	0.70	0.77	0.73
Residues 2–21	1.06	1.74	0.72	0.42	0.29	0.32

identical, as inferred from the similar PRE values observed throughout the peptide sequences. Interestingly, although residues 19–21 are more structured in [K^{8,12},F^{18}]PTC-DA1 than in PTC-B1 with a higher helical propensity, these residues are substantially affected by the gadodiamide probe in both peptides, suggesting that they are positioned close to the water-micelle interface in the two plasticins.

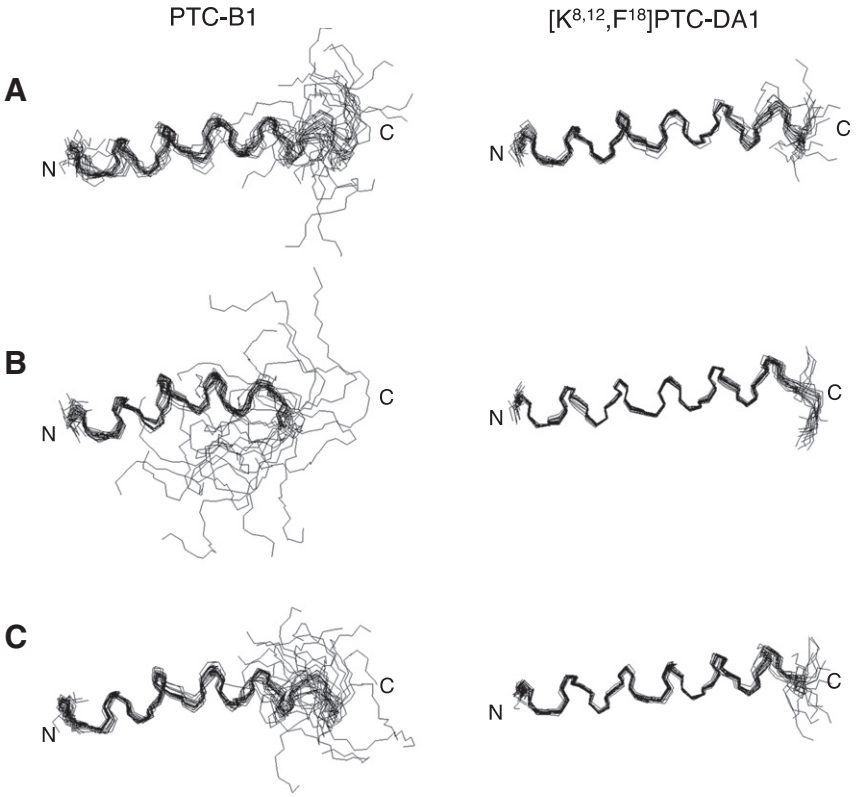

Fig. 4. Three-dimensional NMR structures of PTC-B1 (left) and [K^{8,12},F^{18}]PTC-DA1 (right) in 30% TFE (A), DPC micelles (B), and SDS micelles (C). Structures were superimposed by best fitting of backbone N, Cα and C′ atoms over residues 2–18.

PREs were also measured in the presence of zwitterionic DPC micelles. As shown in Fig. 5B, the paramagnetic waves observed with DPC are highly similar to those obtained with SDS. In both peptides, the helical region 3–18 is embedded within the DPC micelle in a parallel orientation with residues 3, 7, and 10 being the most buried. This indicates that micelle composition has little influence on the orientation and immersion depth of the two plasticins. It should be stressed that the two peptides display smaller PRE values in DPC than in SDS, which can be ascribed to the larger polar head of the DPC detergent in comparison to that of SDS that increases the distance between peptide and the gadodiamide probe.

3.7. Self-associative properties of selected plasticins in the presence of membrane mimetics

Finally, we have used gel electrophoresis to investigate whether plasticins could oligomerize in the presence of detergents or lipid vesicles. SDS-PAGE analysis shows the presence of a unique band corresponding to the monomeric peptides and no band indicative of higher molecular weight oligomers could be observed (Fig. 6, left panels). However, this technique may be inefficient to detect the formation of transient oligomers as such weak non-covalent interactions might be disrupted by SDS detergent [53]. To test this hypothesis, peptide solutions were also preincubated with glutaraldehyde as a cross-linking agent to stabilize putative formed oligomers through covalent bonding [53,54]. Under cross-linking conditions, the bands corresponding to monomeric states remain prominent in both micelles and lipids environments (Fig. 6, right panels). Very weak bands corresponding to dimeric states can be observed in SDS and DMPG anionic environments. Diffuse bands corresponding to higher molecular weight cross-linked species are also distinguishable in the presence of DMPC lipid vesicles, and DMPG to a lesser extent. Altogether, these cross-linking experiments demonstrate that both PTC-B1 and [$K^{8,12}$,F^{18}]PTC-DA1 peptides are mainly monomeric in the various detergent and lipid environments tested.

4. Discussion

This work, together with previous studies, indicates that the two selected PTCs are not structured in water and mainly adopt α-helical conformations in a wide variety of membrane-mimetic environments as diverse as water/TFE mixtures, detergent micelles and lipid vesicles. Thus these cationic PTCs have a high helical propensity in membrane environments and exhibit lower conformational plasticity than neutral or weakly cationic PTCs whose conformational space also encompasses β-sheet structures. Since cationic PTCs are much more efficient in lysing microorganisms membranes than neutral PTCs, it is likely that the membrane-active states of these PTCs have a helical structure.

ITC measurements and helical folding induced by membrane environments demonstrate that PTCs have affinity for both zwitterionic and anionic membranes. This result is in agreement with the observation that PTCs are not only active against microorganisms but are also moderately hemolytic and cytotoxic against a variety of mammalian cells [18]. The interaction of the large hydrophobic face of PTCs with membranes is therefore a major driving force governing peptide

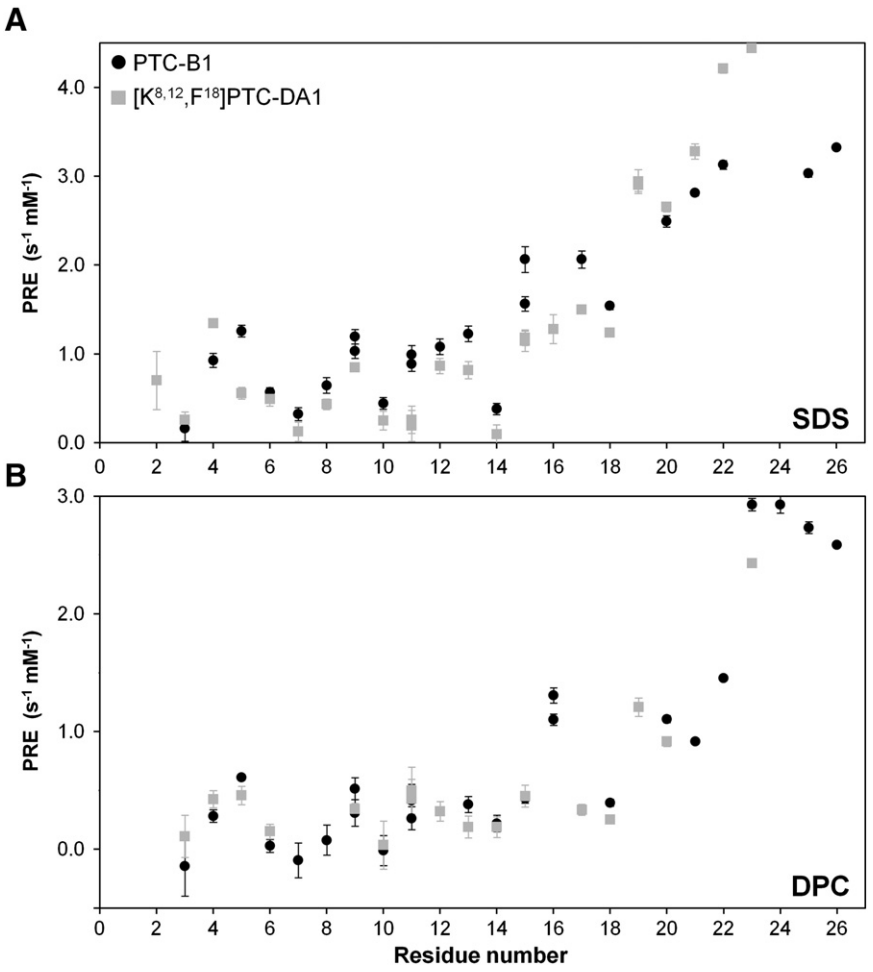

Fig. 5. Use of a paramagnetic reagent to probe the accessibility of plasticin residues in DPC and SDS micelles. Paramagnetic relaxation enhancement rates (PRE) were measured for PTC-B1 (black circles) and [$K^{8,12}$,F^{18}]PTC-DA1 (grey squares) in SDS (A) and DPC (B).

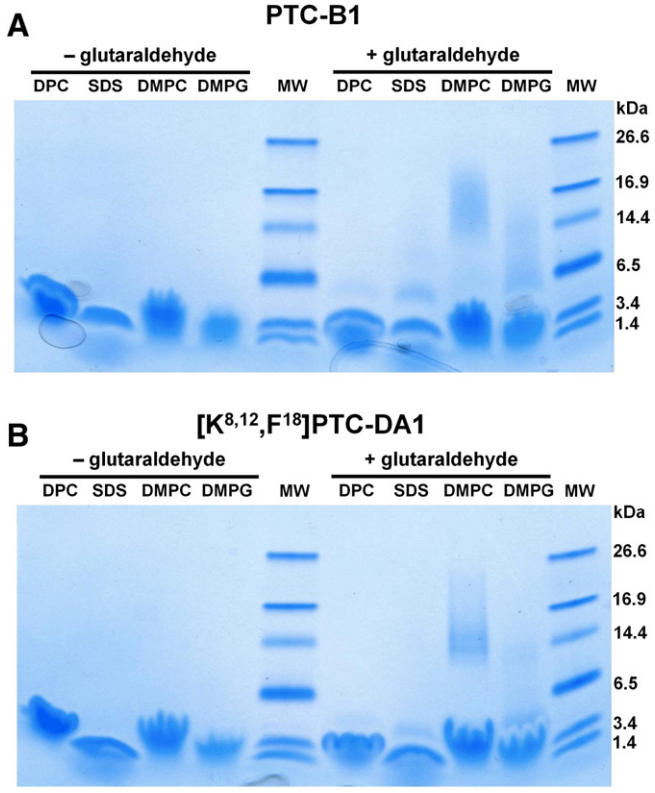

Fig. 6. SDS-PAGE analysis of PTC-B1 (A) and [$K^{8,12}$,F^{18}]PTC-DA1 (B) incubated in micelle or lipid environments in the absence or in the presence of glutaraldehyde cross-linking reagent.

insertion in membranes. The electrostatic interactions between anionic lipids and Lys side chains provide an additional contribution accounting for the differences in affinity, as determined by ITC. As a consequence, the lower helical content of PTCs in DMPC in comparison with DMPG likely reflects the weaker affinities for zwitterionic lipids and proportion of bound states, rather than differences in the helical conformations adopted by membrane-bound states. The diffusion coefficients measured by PFG NMR also shows that PTCs have slightly higher affinities for anionic SDS than for zwitterionic DPC.

The NMR study reveals different helical propensities along the peptide sequence that can be rationalized in terms of amphipathicity, hydrophobicity and distribution of Gly residues. Importantly, the overall conformational preferences tend to be similar in the three investigated media, with only slight differences regarding the C-terminal tail. This indicates that the helical propensities are not strongly affected by the environment. In both PTCs, the N-terminal 1–12 half has a higher helical stability than the C-terminal half, which can be ascribed to a smaller number of Gly residues and the presence of two charged Lys residues that increase the hydrophobic moment of the N-terminal part. Similarly, the higher number of Gly residues in the C-terminal half of PTC-B1 in comparison with [$K^{8,12}$,F^{18}]PTC-DA1 explains the differences in the helical propensities of the two peptides. The α-helices of both PTCs show fraying in the C-terminal region and the last 4 residues of PTC-B1 have no helical propensity which can be accounted for by the lack of hydropathic character of this tail.

Based on the NMR structures calculated at atomic resolution, residues 1–23 of both PTCs are represented on a helical wheel projection (Fig. 7). Leu residues are predominant on the large hydrophobic face that subtends a radial angle of 180°. Gly residues are localized on the polar face and at the junction of both faces. The two cationic Lys residues occupy a small sector with a radial angle of 60°. The location of these residues is completely consistent with NMR PREs. Indeed, NMR positioning experiments shows that the hydrophobic face is buried within micelles and that helix axis lies parallel to the detergent surface. The largest relaxation enhancements in the C-terminal part reflect the lower helical stability and higher accessibility of this region to the water/detergent interface.

Due to the absence of side-chain, Gly residue has an intrinsic conformational flexibility and is classified as a helix-breaker. Indeed, glycine is the residue exhibiting the lowest helical propensity after proline in water-soluble globular proteins. Despite being more abundant in transmembrane helices, glycine has also a low intrinsic helical propensity in membrane environments. Accordingly, glycine residues are often proposed to act as conformational switches by inducing kinks or hinges in the helical structures of antimicrobial peptides, such as dermaseptin B2 [55] or maximin-4 [56,57]. The analysis of PTC-B1 and [$K^{8,12}$,F^{18}]PTC-DA1 NMR structures reveals that the presence of several Gly residues tends to decrease the helical stability. Nevertheless, the repetition of Gly residues does not interrupt the helical conformation of PTCs which remains the major populated state, as shown by the analysis of Cα CSDs, $^3J_{HN\text{-}H\alpha}$ coupling constants and the persistence of medium-range NOEs. PRE measurements indicate that the Gly-rich segments are more sensitive to the paramagnetic probe at the micelle surface, which can be interpreted in terms of increased flexibility and unfolding of the helix. However, the time scale averaging of PRE makes this parameter more sensitive to contributions from transiently populated, minor states. Therefore the PRE analysis does not contradict the structural analysis inferred from other NMR parameters. The comparison of PTC-B1 and [$K^{8,12}$,F^{18}]PTC-DA1 NMR conformational parameters shows that the presence of one glycine residue per helical turn, as observed in [$K^{8,12}$,F^{18}]PTC-DA1, is well accommodated in the helical structure. In contrast, two Gly residues in close positions have a stronger destabilizing effect, as evidenced in PTC-B1 for GG doublet (positions 15,16). The GXG sequence (residues 9–11) is also associated with weaker helical propensities, albeit to a lesser extent.

The absence of significant helix interruption in the Gly-rich segment of the two PTCs may be explained by the specific location of Gly residues that all lie on the polar face of the helix. One reason may be that the absence of side chain should favor the hydration of polar backbone groups on the hydrophilic face. Furthermore, the location of a glycine on the hydrophobic face would be probably more destabilizing since the lack of side chain should be more detrimental to the network of van der Waals interactions between aromatic and aliphatic side chains. Indeed, it was shown that the helical propensity of amino acid in membrane environments is directly related to the side chain hydrophobicity [58]. Such location of Gly on the polar face of α-helices is not specific of PTCs but has been observed for other antimicrobial peptides. For instance, Temporin SHa, despite a Gly content of 23% (3 Gly over 13 residues) also adopts a well-defined amphipathic α-helix in membrane-mimetic environments, all Gly lying on the polar face [59]. Another NMR structure of a Gly-rich PTC, PTC-L1, has recently been determined [15]. In this case, an interruption of the helical structure is clearly observed. Notably, the distribution of Gly markedly differs from that of PTC-B1 and [$K^{8,12}$,F^{18}]PTC-DA1 as they are concentrated in a central loop made mostly of Gly (7 Gly over 8 residues). Therefore the PTCs may be divided into two classes on a structural basis, one forming mostly uninterrupted helices and the other helix-loop-helix structures.

The significance of Gly distribution other repeated GXXXG motifs is not understood but is has been suggested that these motifs could be involved in peptide dimerization. Indeed, the GXXXG motif is frequent in transmembrane helices and plays a role in promoting helix association. Moreover, GXXXG-like motifs are also critical for the function of fusion peptides like HIV-1 fusion peptide [60]. Structural studies on glycophorin dimer and other transmembrane proteins have shown that the small Gly residues favor extensive interhelical van der Waals interactions [61]. The close contact between helices also facilitates the formation of hydrogen bonds between carbonyl and CαH groups. Furthermore, the presence of Gly residues minimizes the entropic cost

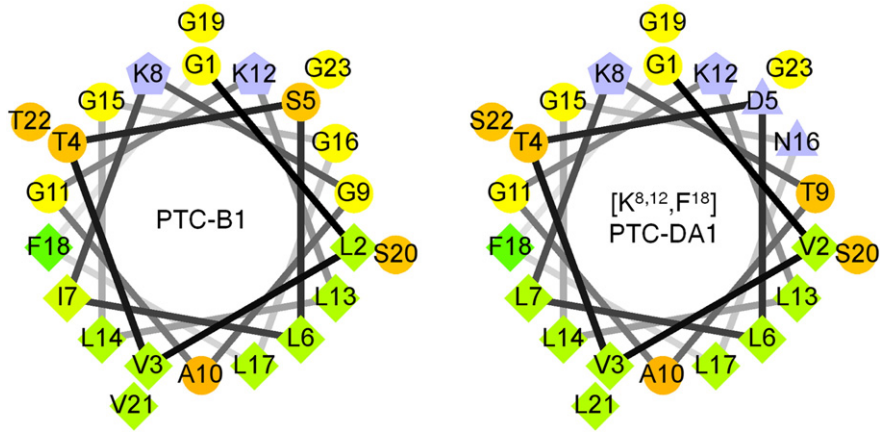

Fig. 7. Helical wheel representation of the 1–23 region of PTC-B1 (left) and [$K^{8,12}$,F^{18}]PTC-DA1 (right). Wheels were generated with wheel.pl (http://rzlab.ucr.edu/scripts/wheel/wheel.cgi).

associated to side-chain conformational restriction at helix interface. In the case of PTCs, we were not able to detect any formation of stable oligomers in detergent micelles by NMR. Indeed, there was no evidence of a monomer/oligomer equilibrium that would be slow on the NMR time scale, as commonly observed for transmembrane helix-helix associations in micelles [62]. Another possibility could be the formation of weak affinity, transient oligomers that would occur in fast exchange on the NMR time scale but such equilibrium is not supported by chemical shifts data that show no concentration dependency. In addition, the formation of a dimerization interface involving Gly residues could not be detected by PRE experiments which revealed that Gly residues are largely exposed to solvent. CD data also provide evidence that both plasticins are mostly monomeric in detergent environments. In particular, the ratio between the intensities of the two characteristic minima at 222 and 208 nm ($\Delta\varepsilon_{222}/\Delta\varepsilon_{208}$), which has been proposed as an indicator of helix oligomerization in coiled coils and transmembrane peptides [63,64], show values around 0.8–0.9, as typically observed for monomeric α-helices. Similar $\Delta\varepsilon_{222}/\Delta\varepsilon_{208}$ ratios are observed in DMPG vesicles (~0.9) while an increase is observed in DMPC vesicles (~1.05), pointing out the presence of some helix-helix association in zwitterionic LUVs. However, no concentration dependency of the $\Delta\varepsilon_{222}/\Delta\varepsilon_{208}$ ratio could be observed in both DMPC and DMPG vesicles upon increase of the peptide/lipid molar ratio from 1/50 to 1/5 (data not shown), suggesting that plasticins are not likely to form stable oligomers in lipid environments. Finally, cross-linking experiments provide additional evidence of weak oligomerization. Gel electrophoresis and the use of a cross-linking agent failed to detect the presence of significant amounts of oligomers in detergent or lipid environments, the observed cross-linked oligomeric states corresponding to low populations. It can be concluded from this study that GXXXG motifs of PTCs do not seem to promote strong association between helices. As a consequence, the involvement of GXXXG motifs in dimerization appears to be strongly dependent on the environment. Notably, the GXXXG motif of the antimicrobial peptide PGLa that is involved in dimerization lies in the hydrophobic sector of the helix [26]. When lying on the hydrophilic face of an amphipathic helix, such GXXXG motif may not drive dimerization as strongly as a similar motif within a hydrophobic membrane environment.

Several studies on antimicrobial peptides have revealed dynamic equilibriums between monomeric and oligomeric states and the transient character of membrane-destabilizing forms [65,66]. It is thus possible that the GXXXG motifs of PTCs may have a more dynamical role in favoring only transient close contacts between helices. Interestingly, these motifs share similarities with amphipathic lipid packing sensor (ALPS) motifs that are made of bulky hydrophobic residues and small polar residues. Such ALPS motifs are involved in membrane curvature sensing by recognizing lipid packing defects [67]. This sequence similarity may suggest an alternative role of GXXXG motifs in PTCs as sensors of membrane curvature, which is regarded as an important parameter in the mechanism of action of interfacial peptides [68].

5. Conclusions

We report for the first time a detailed structural characterization of two cationic plasticins, PTC-B1 and the analog [$K^{8,12}$,F^{18}]PTC-DA1. Both plasticins adopt mainly alpha-helical conformations in a wide variety of membrane-mimicking environments, despite the high content of glycine known to act as a helix breaker residue. Our NMR studies reveal that both PTCs form regular amphipathic α-helices that are oriented parallel to the micelle surface. The Gly residues, arranged in three repeated GXXXG motifs, lye on the solvent-exposed face of the helix. The cationic Lys residues are clustered in a small hydrophilic sector, their electrostatic interaction with anionic membranes enhances membrane binding, as shown by ITC, and is likely to be involved in the discrimination of prokaryotic versus eukaryotic membranes. The large hydrophobic sector made of Leu residues contributes to significant binding to zwitterionic membranes. Combined CD and NMR studies together with biochemical cross-linking data suggest that PTCs are not prone to strong oligomerization, pointing to a different role of GXXXG motifs with respect to those found in transmembrane helices. We propose a structural basis for the low destabilization of helix and weak oligomerization propensity imparted by these GXXXG motifs that is linked to the exclusive location of Gly on the hydrophilic face of the helix. This work forms the basis for a better understanding of structure-function relationships in these membrane-active peptides and has implications for elucidation of the mechanism of action. Cationic plasticins may constitute good starting points for further optimization aiming to generate multifunctional peptides. Indeed, the rational design of optimized entities displaying dual pharmacological properties such as antimicrobial potency together with immunomodulation activity is highly desired with regard to the complexity of targeted diseases.

Acknowledgments

The authors are grateful to Dr Christophe Piesse from the peptidic synthesis service of the IBPS/FR 3631 Institut de Biologie Paris-Seine (Université Pierre and Marie Curie, Paris).

Appendix A. Supplementary data

Supplementary data to this article can be found online at http://dx.doi.org/10.1016/j.bpc.2014.09.004.

References

[1] M. Zasloff, Antimicrobial peptides of multicellular organisms, Nature 415 (2002) 389–395, http://dx.doi.org/10.1038/415389a.
[2] J. Wiesner, A. Vilcinskas, Antimicrobial peptides: the ancient arm of the human immune system, Virulence 1 (2010) 440–464, http://dx.doi.org/10.4161/viru.1.5.12983.
[3] T.L. Pukala, J.H. Bowie, V.M. Maselli, I.F. Musgrave, M.J. Tyler, Host-defence peptides from the glandular secretions of amphibians: structure and activity, Nat. Prod. Rep. 23 (2006) 368–393, http://dx.doi.org/10.1039/b512118n.
[4] J.M. Conlon, Structural diversity and species distribution of host-defense peptides in frog skin secretions, Cell. Mol. Life Sci. 68 (2011) 2303–2315, http://dx.doi.org/10.1007/s00018-011-0720-8.
[5] R.E.W. Hancock, H.-G. Sahl, Antimicrobial and host-defense peptides as new anti-infective therapeutic strategies, Nat. Biotechnol. 24 (2006) 1551–1557, http://dx.doi.org/10.1038/nbt1267.
[6] A.T.Y. Yeung, S.L. Gellatly, R.E.W. Hancock, Multifunctional cationic host defence peptides and their clinical applications, Cell. Mol. Life Sci. 68 (2011) 2161–2176, http://dx.doi.org/10.1007/s00018-011-0710-x.
[7] C.D. Fjell, J.A. Hiss, R.E.W. Hancock, G. Schneider, Designing antimicrobial peptides: form follows function, Nat. Rev. Drug Discov. 11 (2012) 37–51, http://dx.doi.org/10.1038/nrd3591.
[8] C. El Amri, F. Bruston, P. Joanne, C. Lacombe, P. Nicolas, Intrinsic flexibility and structural adaptability of Plasticins membrane-damaging peptides as a strategy for functional versatility, Eur. Biophys. J. 36 (2007) 901–909, http://dx.doi.org/10.1007/s00249-007-0199-2.
[9] M. Amiche, A. Ladram, P. Nicolas, A consistent nomenclature of antimicrobial peptides isolated from frogs of the subfamily Phyllomedusinae, Peptides 29 (2008) 2074–2082, http://dx.doi.org/10.1016/j.peptides.2008.06.017.
[10] D. Vanhoye, F. Bruston, S. El Amri, A. Ladram, M. Amiche, P. Nicolas, Membrane association, electrostatic sequestration, and cytotoxicity of Gly-Leu-rich peptide orthologs with differing functions, Biochemistry 43 (2004) 8391–8409, http://dx.doi.org/10.1021/bi0493158.
[11] J.M. Conlon, Y.H.A. Abdel-Wahab, P.R. Flatt, J. Leprince, H. Vaudry, T. Jouenne, et al., A glycine-leucine-rich peptide structurally related to the plasticins from skin secretions of the frog Leptodactylus laticeps (Leptodactylidae), Peptides 30 (2009) 888–892, http://dx.doi.org/10.1016/j.peptides.2009.01.008.
[12] P. Nicolas, C. El Amri, The dermaseptin superfamily: a gene-based combinatorial library of antimicrobial peptides, Biochim. Biophys. Acta 1788 (2009) 1537–1550, http://dx.doi.org/10.1016/j.bbamem.2008.09.006.
[13] D. Vanhoye, F. Bruston, P. Nicolas, M. Amiche, Antimicrobial peptides from hylid and ranin frogs originated from a 150-million-year-old ancestral precursor with a conserved signal peptide but a hypermutable antimicrobial domain, Eur. J. Biochem. 270 (2003) 2068–2081, http://dx.doi.org/10.1046/j.1432-1033.2003.03584.x.
[14] C. El Amri, P. Nicolas, Plasticins: membrane-damaging peptides with "chameleon-like" properties, Cell. Mol. Life Sci. 65 (2008) 895–909, http://dx.doi.org/10.1007/s00018-007-7445-8.
[15] M.A. Scorciapino, G. Manzo, A.C. Rinaldi, R. Sanna, M. Casu, J.M. Pantic, et al., Conformational analysis of the frog skin peptide, plasticin-L1, and its effects on production of proinflammatory cytokines by macrophages, Biochemistry 52 (2013) 7231–7241, http://dx.doi.org/10.1021/bi4008287.
[16] C. El Amri, C. Lacombe, K. Zimmerman, A. Ladram, M. Amiche, P. Nicolas, et al., The plasticins: membrane adsorption, lipid disorders, and biological activity, Biochemistry 45 (2006) 14285–14297, http://dx.doi.org/10.1021/bi060999o.
[17] P. Joanne, M. Falord, O. Chesneau, C. Lacombe, S. Castano, B. Desbat, et al., Comparative study of two plasticins: specificity, interfacial behavior, and bactericidal activity, Biochemistry 48 (2009) 9372–9383, http://dx.doi.org/10.1021/bi901222p.
[18] P. Joanne, C. Galanth, N. Goasdoué, P. Nicolas, S. Sagan, S. Lavielle, et al., Lipid reorganization induced by membrane-active peptides probed using differential scanning calorimetry, Biochim. Biophys. Acta 1788 (2009) 1772–1781, http://dx.doi.org/10.1016/j.bbamem.2009.05.001.
[19] Y. Shai, Mechanism of the binding, insertion and destabilization of phospholipid bilayer membranes by alpha-helical antimicrobial and cell non-selective membrane-lytic peptides, Biochim. Biophys. Acta 1462 (1999) 55–70, http://dx.doi.org/10.1016/S0005-2736(99)00200-X.
[20] W.C. Wimley, K. Hristova, Antimicrobial peptides: successes, challenges and unanswered questions, J. Membr. Biol. 239 (2011) 27–34, http://dx.doi.org/10.1007/s00232-011-9343-0.
[21] W.P. Russ, D.M. Engelman, The GxxxG motif: a framework for transmembrane helix-helix association, J. Mol. Biol. 296 (2000) 911–919, http://dx.doi.org/10.1006/jmbi.1999.3489.
[22] A. Senes, D.E. Engel, W.F. DeGrado, Folding of helical membrane proteins: the role of polar, GxxxG-like and proline motifs, Curr. Opin. Struct. Biol. 14 (2004) 465–479, http://dx.doi.org/10.1016/j.sbi.2004.07.007.
[23] S. Kim, T.-J. Jeon, A. Oberai, D. Yang, J.J. Schmidt, J.U. Bowie, Transmembrane glycine zippers: physiological and pathological roles in membrane proteins, Proc. Natl. Acad. Sci. U. S. A. 102 (2005) 14278–14283, http://dx.doi.org/10.1073/pnas.0501234102.
[24] G. Kleiger, R. Grothe, P. Mallick, D. Eisenberg, GXXXG and AXXXA: common alpha-helical interaction motifs in proteins, particularly in extremophiles, Biochemistry 41 (2002) 5990–5997.
[25] R.W. Glaser, C. Sachse, U.H.N. Dürr, P. Wadhwani, S. Afonin, E. Strandberg, et al., Concentration-dependent realignment of the antimicrobial peptide PGLa in lipid membranes observed by solid-state 19 F-NMR, Biophys. J. 88 (2005) 3392–3397, http://dx.doi.org/10.1529/biophysj.104.056424.
[26] J.P. Ulmschneider, J.C. Smith, M.B. Ulmschneider, A.S. Ulrich, E. Strandberg, Reorientation and dimerization of the membrane-bound antimicrobial peptide PGLa from microsecond all-atom MD simulations, Biophys. J. 103 (2012) 472–482, http://dx.doi.org/10.1016/j.bpj.2012.06.040.
[27] C. Oppegård, J. Schmidt, P.E. Kristiansen, J. Nissen-Meyer, Mutational analysis of putative helix-helix interacting GxxxG-motifs and tryptophan residues in the two-peptide bacteriocin lactococcin G, Biochemistry 47 (2008) 5242–5249, http://dx.doi.org/10.1021/bi800289w.
[28] K. Zangger, R. Gössler, L. Khatai, K. Lohner, A. Jilek, Structures of the glycine-rich diastereomeric peptides bombinin H2 and H4, Toxicon 52 (2008) 246–254, http://dx.doi.org/10.1016/j.toxicon.2008.05.011.
[29] G. Rouser, S. Fleischer, A. Yamamoto, Two dimensional thin layer chromatographic separation of polar lipids and determination of phospholipids by phosphorus analysis of spots, Lipids 5 (1970) 494–496, http://dx.doi.org/10.1007/BF02531316.
[30] L. Zhong, W.C. Johnson, Environment affects amino acid preference for secondary structure, Proc. Natl. Acad. Sci. U. S. A. 89 (1992) 4462–4465, http://dx.doi.org/10.1073/pnas.89.10.4462.
[31] C. Bartels, T. Xia, M. Billeter, P. Güntert, K. Wüthrich, The program XEASY for computer-supported NMR spectral analysis of biological macromolecules, J. Biomol. NMR 6 (1995) 1–10, http://dx.doi.org/10.1007/BF00417486.
[32] T.D. Goddard, D.G. Kneller, SPARKY 3, University of California, San Francisco, (n.d.).
[33] D.S. Wishart, C.G. Bigam, A. Holm, R.S. Hodges, B.D. Sykes, 1H, 13C and 15 N random coil NMR chemical shifts of the common amino acids. I. Investigations of nearest-neighbor effects, J. Biomol. NMR 5 (1995) 67–81.
[34] T. Szyperski, P. Güntert, G. Otting, K. Wüthrich, Determination of scalar coupling constants by inverse Fourier transformation of in-phase multiplets, J. Magn. Reson. 99 (1992) 552–560, http://dx.doi.org/10.1016/0022-2364(92)90209-P.
[35] D.H. Wu, A.D. Chen, C.S. Johnson, An improved diffusion-ordered spectroscopy experiment incorporating bipolar-gradient pulses, J. Magn. Reson. A 115 (1995) 260–264, http://dx.doi.org/10.1006/jmra.1995.1176.
[36] F. Delaglio, S. Grzesiek, G.W. Vuister, G. Zhu, J. Pfeifer, A. Bax, NMRPipe: a multidimensional spectral processing system based on UNIX pipes, J. Biomol. NMR 6 (1995) 277–293, http://dx.doi.org/10.1007/BF00197809.
[37] P. Stilbs, Micellar breakdown by short-chain alcohols. A multicomponent FT-PGSE-NMR self-diffusion study, J. Colloid Interface Sci. 89 (1982) 547–554.
[38] B. Lindman, N. Kamenka, M.C. Puyal, B. Brun, B. Joensson, Tracer self-diffusion studies of micelle formation of a short-chain ionic surfactant, sodium n-octanoate, J. Phys. Chem. 88 (1984) 53–57, http://dx.doi.org/10.1021/j150645a013.
[39] T.L. Whitehead, L.M. Jones, R.P. Hicks, PFG-NMR investigations of the binding of cationic neuropeptides to anionic and zwitterionic micelles, J. Biomol. Struct. Dyn. 21 (2004) 567–576, http://dx.doi.org/10.1080/07391102.2004.10506949.
[40] Y. Shen, F. Delaglio, G. Cornilescu, A. Bax, TALOS+: a hybrid method for predicting protein backbone torsion angles from NMR chemical shifts, J. Biomol. NMR 44 (2009) 213–223, http://dx.doi.org/10.1007/s10858-009-9333-z.
[41] Y. Shen, A. Bax, Protein backbone and sidechain torsion angles predicted from NMR chemical shifts using artificial neural networks, J. Biomol. NMR 56 (2013) 227–241, http://dx.doi.org/10.1007/s10858-013-9741-y.
[42] P. Güntert, C. Mumenthaler, K. Wüthrich, Torsion angle dynamics for NMR structure calculation with the new program DYANA, J. Mol. Biol. 273 (1997) 283–298, http://dx.doi.org/10.1006/jmbi.1997.1284.
[43] C.D. Schwieters, J.J. Kuszewski, N. Tjandra, G.M. Clore, The Xplor-NIH NMR molecular structure determination package, J. Magn. Reson. 160 (2003) 65–73, http://dx.doi.org/10.1016/S1090-7807(02)00014-9.
[44] R.A. Laskowski, J.A. Rullmannn, M.W. MacArthur, R. Kaptein, J.M. Thornton, AQUA and PROCHECK-NMR: programs for checking the quality of protein structures solved by NMR, J. Biomol. NMR 8 (1996) 477–486, http://dx.doi.org/10.1007/BF00228148.
[45] J. Seelig, Thermodynamics of lipid-peptide interactions, Biochim. Biophys. Acta 1666 (2004) 40–50, http://dx.doi.org/10.1016/j.bbamem.2004.08.004.
[46] V.V. Andrushchenko, M.H. Aarabi, L.T. Nguyen, E.J. Prenner, H.J. Vogel, Thermodynamics of the interactions of tryptophan-rich cathelicidin antimicrobial peptides with model and natural membranes, Biochim. Biophys. Acta 1778 (2008) 1004–1014, http://dx.doi.org/10.1016/j.bbamem.2007.12.022.
[47] A. Walrant, A. Vogel, I. Correia, O. Lequin, B.E.S. Olausson, B. Desbat, et al., Membrane interactions of two arginine-rich peptides with different cell internalization capacities, Biochim. Biophys. Acta Biomembr. 1818 (2012) 1755–1763, http://dx.doi.org/10.1016/j.bbamem.2012.02.024.
[48] K.A. Brogden, Antimicrobial peptides: pore formers or metabolic inhibitors in bacteria? Nat. Rev. Microbiol. 3 (2005) 238–250, http://dx.doi.org/10.1038/nrmicro1098.
[49] E.F. Haney, H.N. Hunter, K. Matsuzaki, H.J. Vogel, Solution NMR studies of amphibian antimicrobial peptides: linking structure to function? Biochim. Biophys. Acta 1788 (2009) 1639–1655, http://dx.doi.org/10.1016/j.bbamem.2009.01.002.
[50] M. Respondek, T. Madl, C. Göbl, R. Golser, K. Zangger, Mapping the orientation of helices in micelle-bound peptides by paramagnetic relaxation waves, J. Am. Chem. Soc. 129 (2007) 5228–5234, http://dx.doi.org/10.1021/ja069004f.
[51] E. Schrank, G.E. Wagner, K. Zangger, Solution NMR studies on the orientation of membrane-bound peptides and proteins by paramagnetic probes, Molecules 18 (2013) 7407–7435, http://dx.doi.org/10.3390/molecules18077407.
[52] L. Carlier, S. Balayssac, F.-X. Cantrelle, L. Khemtémourian, G. Chassaing, A. Joliot, et al., Investigation of homeodomain membrane translocation properties: insights from the structure determination of engrailed-2 homeodomain in aqueous and membrane-mimetic environments, Biophys. J. 105 (2013) 667–678, http://dx.doi.org/10.1016/j.bpj.2013.06.024.
[53] R. Saravanan, S. Bhattacharjya, Oligomeric structure of a cathelicidin antimicrobial peptide in dodecylphosphocholine micelle determined by NMR spectroscopy,

Biochim. Biophys. Acta 1808 (2011) 369–381, http://dx.doi.org/10.1016/j.bbamem.2010.10.001.
[54] Y. Zhang, L. Wang, Y. Hu, C. Jin, Solution structure of the TatB component of the twin-arginine translocation system, Biochim. Biophys. Acta 1838 (2014) 1881–1888, http://dx.doi.org/10.1016/j.bbamem.2014.03.015.
[55] O. Lequin, F. Bruston, O. Convert, G. Chassaing, P. Nicolas, Helical structure of dermaseptin B2 in a membrane-mimetic environment, Biochemistry 42 (2003) 10311–10323, http://dx.doi.org/10.1021/bi034401d.
[56] O. Toke, Z. Bánóczi, P. Király, R. Heinzmann, J. Bürck, A.S. Ulrich, et al., A kinked antimicrobial peptide from Bombina maxima. I. Three-dimensional structure determined by NMR in membrane-mimicking environments, Eur. Biophys. J. 40 (2011) 447–462, http://dx.doi.org/10.1007/s00249-010-0657-0.
[57] R. Heinzmann, S.L. Grage, C. Schalck, J. Bürck, Z. Bánóczi, O. Toke, et al., A kinked antimicrobial peptide from Bombina maxima. II. Behavior in phospholipid bilayers, Eur. Biophys. J. 40 (2011) 463–470, http://dx.doi.org/10.1007/s00249-010-0668-x.
[58] S.C. Li, C.M. Deber, A measure of helical propensity for amino acids in membrane environments, Nat. Struct. Biol. 1 (1994) 368–373, http://dx.doi.org/10.1038/nsb0694-368.
[59] F. Abbassi, C. Galanth, M. Amiche, K. Saito, C. Piesse, L. Zargarian, et al., Solution structure and model membrane interactions of temporins-SH, antimicrobial peptides from amphibian skin. A NMR spectroscopy and differential scanning calorimetry study, Biochemistry 47 (2008) 10513–10525, http://dx.doi.org/10.1021/bi8006884.
[60] O. Faingold, T. Cohen, Y. Shai, A GxxxG-like motif within HIV-1 fusion peptide Is critical to its immunosuppressant activity, structure, and interaction with the transmembrane domain of the T-cell receptor, J. Biol. Chem. 287 (2012) 33503–33511, http://dx.doi.org/10.1074/jbc.M112.370817.
[61] K.R. MacKenzie, J.H. Prestegard, D.M. Engelman, A transmembrane helix dimer: structure and implications, Science 276 (1997) 131–133, http://dx.doi.org/10.1126/science.276.5309.131.
[62] K.S. Mineev, D.M. Lesovoy, D.R. Usmanova, S.A. Goncharuk, M.A. Shulepko, E.N. Lyukmanova, et al., NMR-based approach to measure the free energy of transmembrane helix-helix interactions, Biochim. Biophys. Acta 1838 (2014) 164–172, http://dx.doi.org/10.1016/j.bbamem.2013.08.021.
[63] M. Nomizu, A. Utani, K. Beck, A. Otaka, P.P. Roller, Y. Yamada, Mechanism of laminin chain assembly into a triple-stranded coiled-coil structure, Biochemistry 35 (1996) 2885–2893, http://dx.doi.org/10.1021/bi951555n.
[64] L. Khemtémourian, S. Buchoux, F. Aussenac, E.J. Dufourc, Dimerization of Neu/Erb2 transmembrane domain is controlled by membrane curvature, Eur. Biophys. J. 36 (2007) 107–112, http://dx.doi.org/10.1007/s00249-006-0111-5.
[65] M.P. dos Santos Cabrera, D.S. Alvares, N.B. Leite, B. Monson de Souza, M.S. Palma, K. A. Riske, et al., New insight into the mechanism of action of wasp mastoparan peptides: lytic activity and clustering observed with giant vesicles, Langmuir 27 (2011) 10805–10813, http://dx.doi.org/10.1021/la202608r.
[66] A.J. Krauson, J. He, W.C. Wimley, Determining the mechanism of membrane permeabilizing peptides: identification of potent, equilibrium pore-formers, Biochim. Biophys. Acta 1818 (2012) 1625–1632, http://dx.doi.org/10.1016/j.bbamem.2012.02.009.
[67] S. Vanni, L. Vamparys, R. Gautier, G. Drin, C. Etchebest, P.F.J. Fuchs, et al., Amphipathic lipid packing sensor motifs: probing bilayer defects with hydrophobic residues, Biophys. J. 104 (2013) 575–584, http://dx.doi.org/10.1016/j.bpj.2012.11.3837.
[68] D. Koller, K. Lohner, The role of spontaneous lipid curvature in the interaction of interfacially active peptides with membranes, Biochim. Biophys. Acta 1838 (2014) 2250–2259, http://dx.doi.org/10.1016/j.bbamem.2014.05.013.